How Realistic is Photorealistic?

Siwei Lyu and Hany Farid

***Abstract*—Computer graphics rendering software is capable of generating highly photorealistic images that can be impossible to differentiate from photographic images. As a result, the unique stature of photographs as a definitive recording of events is being diminished (the ease with which digital images can be manipulated is, of course, also contributing to this demise). To this end, we describe a method for differentiating between photorealistic and photographic images. Specifically, we show that a statistical model based on first-order and higher order wavelet statistics reveals subtle but significant differences between photorealistic and photographic images.**

***Index Terms*—Digital forensics, image statistics, photorealism.**

I. Introduction

SOPHISTICATED computer graphics rendering software can generate remarkably photorealistic images. Though it may take some effort, photorealistic images can be created that are nearly impossible to differentiate from photographic images. As the rendering technology improves, photorealistic images will become increasingly easier to generate and more realistic.

This technology is already having direct implications on our society. For example, in 1996 the United States Congress passed The Child Pornography Prevention Act which, in part, prohibited any image that *appears to be* or *conveys the impression of* someone under 18 engaged in sexually explicit conduct. This law made illegal computer generated pictures that only appear to show minors involved in sexual activity. In 2002, however, the United States Supreme Court struck down this law in their 6–3 ruling in *Ashcroft Versus Free Speech Coalition*. The court said that language in the 1996 child pornography law was unconstitutionally vague and far-reaching. This ruling makes it considerably more difficult for law enforcement agencies to prosecute child pornography crimes, since it is always possible to claim that any image is computer generated.

If we are to have any hope that photographs will again hold the unique stature of being a definitive recording of events, we must develop technology that can differentiate between photographic and photorealistic images. There has been some work in evaluating the photorealism of computer graphics rendered images from a human perception point of view (e.g., [9]–[11]). To our knowledge, however, no computational techniques exist to differentiate between photographic and photorealistic images (a method for differentiating between photographic and (nonrealistic) graphical icons was proposed in [1]). Related work, though probably not directly applicable, include techniques to differentiate between city and landscape images [14], [16], indoor and outdoor images [13], and photographs and paintings [4].

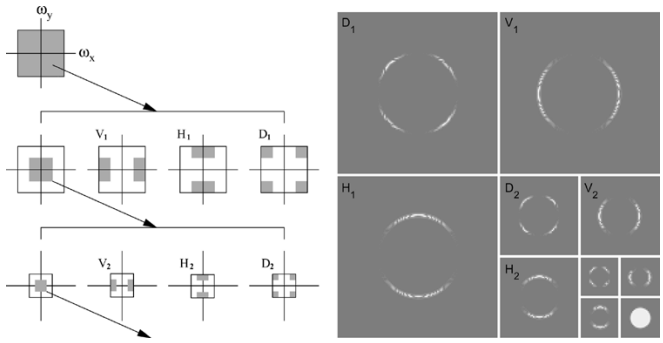

Fig. 1. (Left) Idealized multiscale and orientation decomposition of frequency space. (Top to bottom) Levels 0, 1, and 2. (Left to right) Low-pass, vertical, horizontal, and diagonal subbands. (Right) Magnitude of a multiscale and orientation decomposition of a "disc" image.

In this paper, we describe a statistical model for photographic images that is built upon a wavelet-like decomposition. The model consists of first-order and higher order statistics that capture regularities that are inherent to photographic images. We then show that this model can be used to differentiate between photographic and photorealistic images—from a database of 40 000 photographic and 6000 photorealistic images, we correctly classify approximately 67% of the photorealistic images while only misclassifying 1% of the photographic images. We have previously used a similar technique to detect messages hidden within digital images (steganography) [7], [8].

II. Statistical Model

The decomposition of images using basis functions that are localized in spatial position, orientation, and scale (e.g., wavelet) have proven extremely useful in image compression, image coding, noise removal, and texture synthesis. One reason is that such decompositions exhibit statistical regularities that can be exploited. The image decomposition employed here is based on separable quadrature mirror filters (QMFs) [12], [15], [18]. As illustrated in Fig. 1, this decomposition splits the frequency space into multiple scales, and orientations (a vertical, a horizontal, and a diagonal subband). For a color (RGB) image, the decomposition is applied independently to each color channel. The resulting vertical, horizontal, and diagonal

Manuscript received April 8, 2004; revised October 11, 2004. This work was supported by an A. P. Sloan Fellowship, by National Science Foundation (NSF) CAREER Award IIS99-83806, by NSF Infrastructure Grant EIA-98-02068, and under Award 2000-DT-CX-K001 from the Office for Domestic Preparedness, U.S. Department of Homeland Security (points of view in this document are those of the authors and do not necessarily represent the official position of the U.S. Department of Homeland Security). The associate editor coordinating the review of this manuscript and approving it for publication was Prof. Pierre Moulin.

The authors are with the Computer Science Department, Dartmouth College, Hanover, NH 03755 USA (e-mail: lsw@cs.dartmouth.edu; farid@cs.dartmouth.edu).

Digital Object Identifier 10.1109/TSP.2004.839896

subbands for scale i are denoted as $V_i^c(x,y)$, $H_i^c(x,y)$, and $D_i^c(x,y)$ respectively, where $c \in \{r,g,b\}$.

Wavelet subband coefficients for natural images typically follow a distribution which is well modeled by a generalized Laplacian $P(x) = (1/Z)e^{-|x/s|^p}$, where s,p are the density parameters, and Z is a normalizing constant [2]. This family of densities are characterized by a sharp peak at zero and large symmetric tails. An intuitive explanation for this is that natural images typically contain large smooth regions and abrupt transitions (e.g., edges). The smooth regions, though dominant, produce small coefficients near zero, while the transitions generate large coefficients. In our statistical model, instead of directly estimating the generalized Lapalacian distribution, a simpler approach is taken to characterize these marginal distributions. More specifically, the first four order statistics (mean, variance, skewness, and kurtosis) of the subband coefficient histograms at each orientation, scale, and color channel are collected. These statistics form the first half of our statistical model.

While these statistics describe the basic coefficient distributions, they are unlikely to capture the strong correlations that exist across space, orientation, and scale [2], [6]. For example, salient image features such as edges tend to orient spatially in certain direction and extend across multiple scales. These image features result in substantial local energy across many scales, orientations, and spatial locations. The local energy can be roughly measured by the magnitude of the decomposition coefficient. As such, a strong coefficient in a horizontal subband may indicate that its left and right spatial neighbors in the same subband will also have a large value. Similarly, if there is a coefficient with large magnitude at scale i, it is also very likely that its "parent" at scale $i+1$ will also have a large magnitude.

In order to capture some of these higher order statistical correlations, we collect a second set of statistics that are based on the errors in a linear predictor of coefficient magnitude [2]. For the purpose of illustration, consider first a vertical band of the green channel at scale i, $V_i^g(x,y)$. A linear predictor for the magnitude of these coefficients in a subset[1] of all possible spatial, orientation, scale, and color neighbors is given by

$$\begin{aligned}|V_i^g(x,y)| = {} & w_1|V_i^g(x-1,y)| + w_2|V_i^g(x+1,y)| \\ & + w_3|V_i^g(x,y-1)| + w_4|V_i^g(x,y+1)| \\ & + w_5\left|V_{i+1}^g\left(\frac{x}{2},\frac{y}{2}\right)\right| + w_6|D_i^g(x,y)| \\ & + w_7\left|D_{i+1}^g\left(\frac{x}{2},\frac{y}{2}\right)\right| + w_8|V_i^r(x,y)| \\ & + w_9|V_i^b(x,y)| \end{aligned} \tag{1}$$

where $|\cdot|$ denotes absolute value and w_k are the scalar weights. This linear relationship can be expressed more compactly in matrix form as

$$\vec{v} = Q\vec{w} \tag{2}$$

where $\vec{v}$ contains the coefficient magnitudes of $V_i^g(x,y)$ strung out into a column vector (to reduce sensitivity to noise, only magnitudes greater than 1 are considered), the columns of the matrix Q contain the neighboring coefficient magnitudes as specified in (1), and $\vec{w} = (w_1 \quad \ldots \quad w_9)^T$. The weights $\vec{w}$ are determined by minimizing the following quadratic error function:

$$E(\vec{w}) = [\vec{v} - Q\vec{w}]^2. \tag{3}$$

This error function is minimized by differentiating with respect to $\vec{w}$

$$\frac{dE(\vec{w})}{d\vec{w}} = 2Q^T(\vec{v} - Q\vec{w}) \tag{4}$$

setting the result equal to zero, and solving for $\vec{w}$ to yield

$$\vec{w} = (Q^TQ)^{-1}Q^T\vec{v}. \tag{5}$$

Given the large number of constraints (one per pixel) in only nine unknowns, it is generally safe to assume that the 9×9 matrix Q^TQ will be invertible.

Given the linear predictor, the log error between the actual coefficient and the predicted coefficient magnitudes is

$$\vec{p} = \log(\vec{v}) - \log(|Q\vec{w}|) \tag{6}$$

where the $\log(\cdot)$ is computed point-wise on each vector component. As with the coefficient statisics, mean, variance, skewness, and kurtosis of this error distribution are collected. This process is repeated for scales $i = 1, \ldots, n-1$, and for the subbands V_i^r and V_i^b, where the linear predictors for these subbands are of the form

$$\begin{aligned}|V_i^r(x,y)| = {} & w_1|V_i^r(x-1,y)| + w_2|V_i^r(x+1,y)| \\ & + w_3|V_i^r(x,y-1)| + w_4|V_i^r(x,y+1)| \\ & + w_5|V_{i+1}^r\left(\frac{x}{2},\frac{y}{2}\right)| + w_6|D_i^r(x,y)| \\ & + w_7|D_{i+1}^r\left(\frac{x}{2},\frac{y}{2}\right)| + w_8|V_i^g(x,y)| \\ & + w_9|V_i^b(x,y)| \end{aligned} \tag{7}$$

and

$$\begin{aligned}|V_i^b(x,y)| = {} & w_1|V_i^b(x-1,y)| + w_2|V_i^b(x+1,y)| \\ & + w_3|V_i^b(x,y-1)| + w_4|V_i^b(x,y+1)| \\ & + w_5|V_{i+1}^b\left(\frac{x}{2},\frac{y}{2}\right)| + w_6|D_i^b(x,y)| \\ & + w_7|D_{i+1}^b\left(\frac{x}{2},\frac{y}{2}\right)| + w_8|V_i^r(x,y)| \\ & + w_9|V_i^g(x,y)|. \end{aligned} \tag{8}$$

A similar process is repeated for the horizontal and diagonal subbands. As an example, the predictor for the green channel takes the form

$$\begin{aligned}|H_i^g(x,y)| = {} & w_1|H_i^g(x-1,y)| + w_2|H_i^g(x+1,y)| \\ & + w_3|H_i^g(x,y-1)| + w_4|H_i^g(x,y+1)| \\ & + w_5\left|H_{i+1}^g\left(\frac{x}{2},\frac{y}{2}\right)\right| + w_6|D_i^g(x,y)| \\ & + w_7\left|D_{i+1}^g\left(\frac{x}{2},\frac{y}{2}\right)\right| + w_8|H_i^r(x,y)| \\ & + w_9|H_i^b(x,y)| \end{aligned} \tag{9}$$

[1]The particular choice of neighbors was motivated by the observations of [2] and modified to include noncasual neighbors.

and

$$\begin{aligned}|D_i^g(x,y)| = {} & w_1|D_i^g(x-1,y)| + w_2|D_i^g(x+1,y)| \\ & + w_3|D_i^g(x,y-1)| + w_4|D_i^g(x,y+1)| \\ & + w_5\left|D_{i+1}^g\left(\frac{x}{2},\frac{y}{2}\right)\right| + w_6|H_i^g(x,y)| \\ & + w_7|V_i^g(x,y)| + w_8|D_i^r(x,y)| \\ & + w_9|D_i^b(x,y)|. \end{aligned} \tag{10}$$

For the horizontal and diagonal subbands, the predictor for the red and blue channels are determined in a similar way as was done for the vertical subbands [see (7) and (8)]. For each oriented, scale, and color subband, a similar error metric (6) and error statistics are computed.

For a multiscale decomposition with scales $i = 1, \ldots, n$, the total number of basic coefficient statistics is $36(n-1)$ ($12(n-1)$ per color channel), and the total number of error statistics is also $36(n-1)$, yielding a grand total of $72(n-1)$ statistics. These statistics form the feature vector to be used to discriminate between photorealistic and photographic images.

III. Classification

From the measured statistics of a training set of images labeled as photorealistic or photographic, our goal is to build a classifier that can determine to which category a novel test image belongs.

To this end, linear discrimination analysis (LDA) is a widely used classification algorithm [5]. In a two-class LDA, a one-dimensional linear subspace is found such that when the features are projected onto this subspace, the within-class scatter is minimized while the between-class scatter is maximized. LDA is attractive because of its general effectiveness and simplicity (the classifier is built using a closed-form generalized eigenvector solution). The drawback of LDA is that the classification surface is constrained to be linear.

Support vector machines (SVM) afford a more flexible nonlinear classification surface [17]. Within this family of classifiers there are both linear and nonlinear SVMs. A linear SVM is similar to an LDA, the difference being in the objective function that is minimized. A nonlinear SVM extends a linear SVM by using a kernel function to map the training exemplars into a higher (possibly infinite) dimensional space. While affording a more flexible classifier, the construction of a nonlinear SVM is no longer closed-form, but requires an iterative numerical optimization.

We employed both LDA and a nonlinear SVM for the purposes of distinguishing between photorealistic and photographic images.

IV. Results

Shown in Figs. 2 and 3 are several images taken from a database of 40 000 photographic and 6000 photorealistic images.[2] All of the images consist of a broad range of indoor and outdoor scenes, and the photorealistic images were rendered using a number of different software packages (e.g., 3D Studio Max, Maya, SoftImage 3D, PovRay, Lightwave 3D, and Imagine). All of the images are color (RGB), JPEG compressed (with an average quality of 90%), and typically on the order of 600×400 pixels in size.

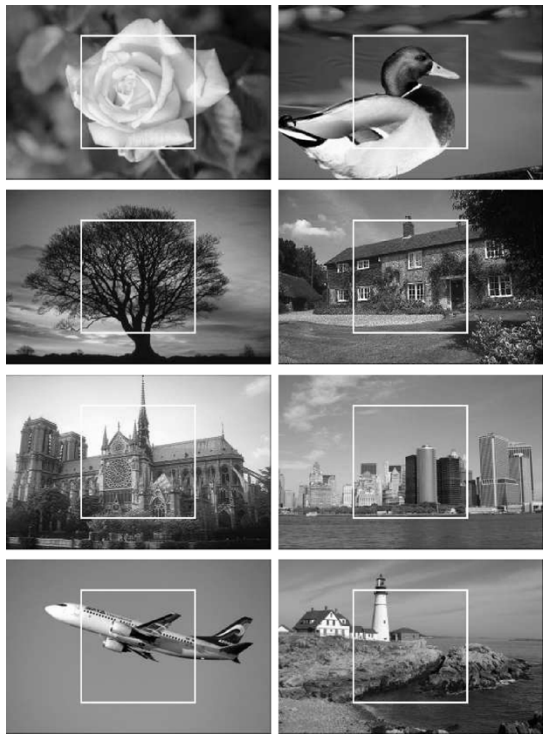

Fig. 2. Eight examples from a database of 40 000 photographic images. The central 256×256 white boxes denote the region of the image from which statistics are measured.

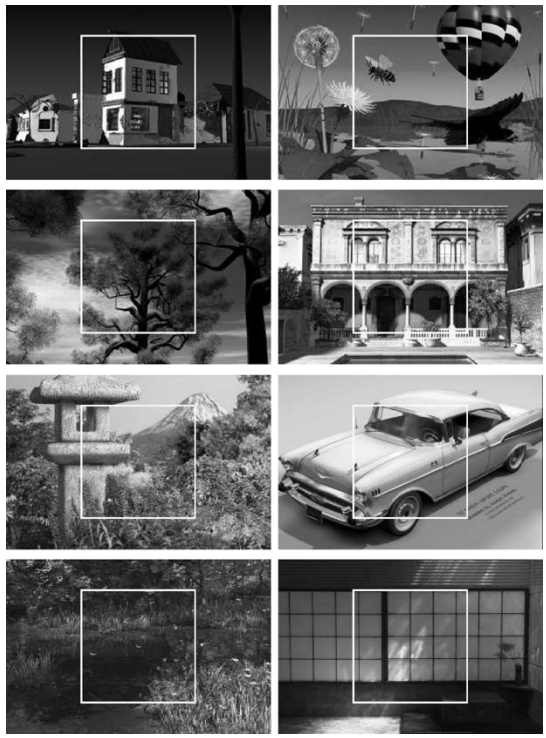

Fig. 3. Eight examples from a database of 6000 photorealistic images. The central 256×256 white boxes denote the region of the image from which statistics are measured.

[2]The photographic images were downloaded from www.freefoto.com, the photorealistic images were downloaded from www.raph.com and www.irtc.org.

TABLE I
CLASSIFICATION RESULTS USING LDA AND SVM. SHOWN ARE THE AVERAGE ACCURACIES (IN PERCENT) OVER 100 RANDOM TRAINING/TESTING SPLITS OF THE DATABASE OF 40 000 PHOTOGRAPHIC AND 6000 PHOTOREALISTIC IMAGES

	training		testing	
	LDA	SVM	LDA	SVM
photographic	58.7	70.9	54.6	66.8
photorealistic	99.4	99.1	99.2	98.8

From this database of 46 000 images, statistics as described in Section II were extracted. To accommodate different image sizes, only the central 256×256 region of each image was considered. For each image region, a four-level three-orientation QMF pyramid[3] was constructed for each color channel, from which a 216-dimensional feature vector (72 per color channel) of coefficient and error statistics was collected.

From the 46 000 feature vectors, 32 000 photographic and 4800 photorealistic feature vectors were used to train both an LDA and a nonlinear SVM.[4] The remaining feature vectors were used to test the classifiers. In the results presented here, the training/testing split was done randomly. We report, in Table I, the classification accuracy over 100 such splits. With a 0.8% false-negative rate (a photorealistic image classified as photographic), the LDA correctly classified approximately 54.6% of the photorealistic images. A nonlinear SVM had better performance, correctly classifying approximately 66.8% of the photographic images, with a 1.2% false-negative rate. Note that in both cases the testing accuracy was fairly close to the training accuracy, suggesting that the classifiers generalized.

We next wondered which images were most easy and most difficult to classify. Specifically, images that are easy to classify are those that are far from the separating classification surface, and those that are hard to classify are near, or on the wrong side of, the classification surface. Shown in Figs. 4 and 5 are eight photographic images and eight photorealistic images, respectively, that were easily classified under the nonlinear SVM. We found that photographic images of trees, plants, etc. are particularly easy to classify, but note that city scenes are also correctly classified. We also noticed that photorealistic images that are easy to classify appear to be particularly artificial (e.g., lack of depth-of-field, lack of details, plastic appearance, etc.). Shown in Fig. 6 are eight photographic images that were incorrectly classified as photorealistic, and shown in Fig. 7 are eight photorealistic images incorrectly classified as photographic. Note that several of the incorrectly classified photographic images consist of road signs and one is of a painting.

We further tested the RBF SVM classifier on a novel set of 14 images (seven photographic, seven photorealistic) from the

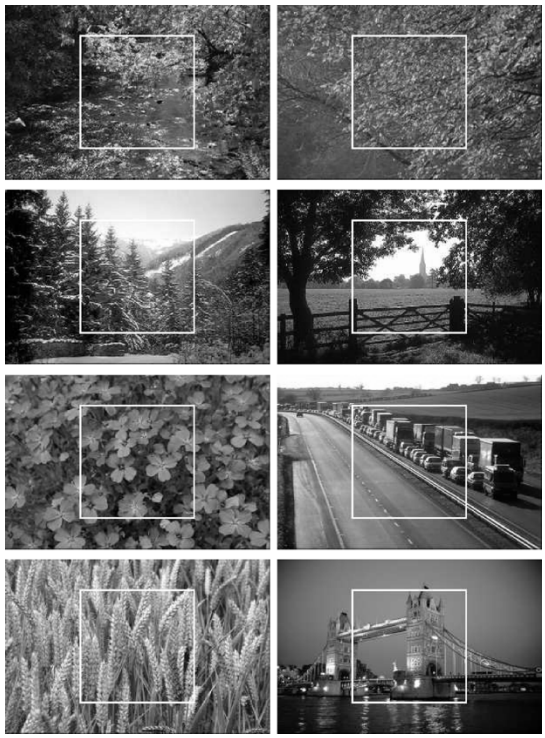

Fig. 4. Easily classified photographic images.

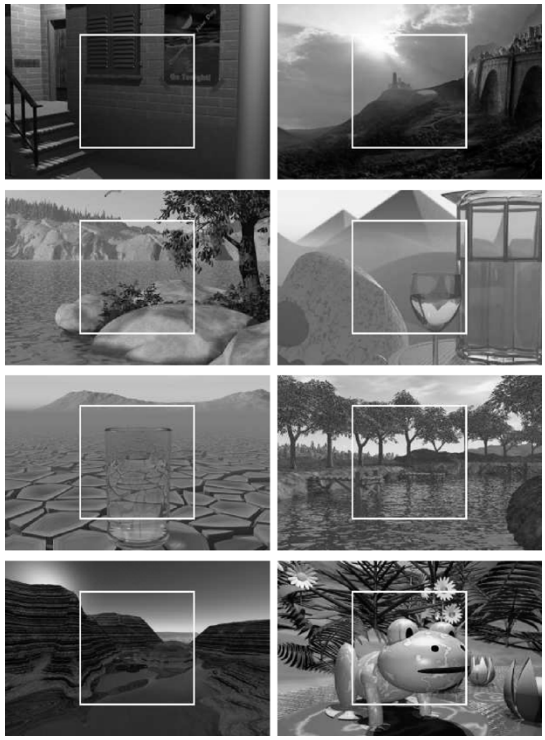

Fig. 5. Easily classified photorealistic images.

[3]We employed a 9-tap QMF filter as the basis of the multiscale multiorientation image decomposition. The low-pass (l) and high-pass (h) filters are given by

$$l = [0.028\,073\,82 \; -0.060\,944\,743 \; -0.073\,386\,624 \; 0.414\,725\,45 \; 0.797\,393\,4 \; 0.414\,725\,45 \; -0.073\,386\,624 \; -0.060\,944\,743 \; 0.028\,073\,82]$$

$$h = [0.028\,073\,82 \; 0.060\,944\,743 \; -0.073\,386\,624 \; -0.414\,725\,45 \; 0.797\,393\,4 \; -0.414\,725\,45 \; -0.073\,386\,624 \; 0.060\,944\,743 \; 0.028\,073\,82].$$

We have also experimented with both Laplacian and steerable pyramid decompositions. Results from a steerable pyramid (with eight orientation subbands) were similar to the results using a QMF pyramid (which use only three orientation subbands). The Laplacian pyramid generally gave poor results. So while it seems that oriented subbands are necessary, it also seems that a finer orientation tuning is not necessary for this particular task.

[4]We employed the SVM algorithm implemented in LIBSVM [3], along with an RBF kernel.

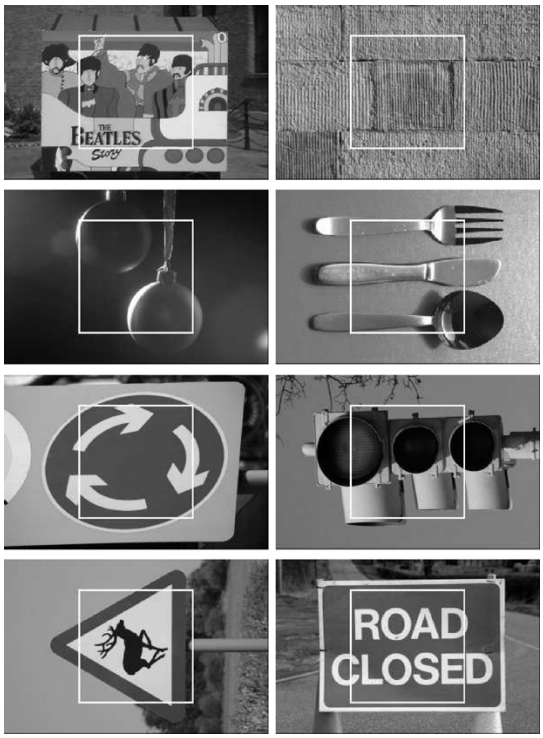

Fig. 6. Incorrectly classified photographic images.

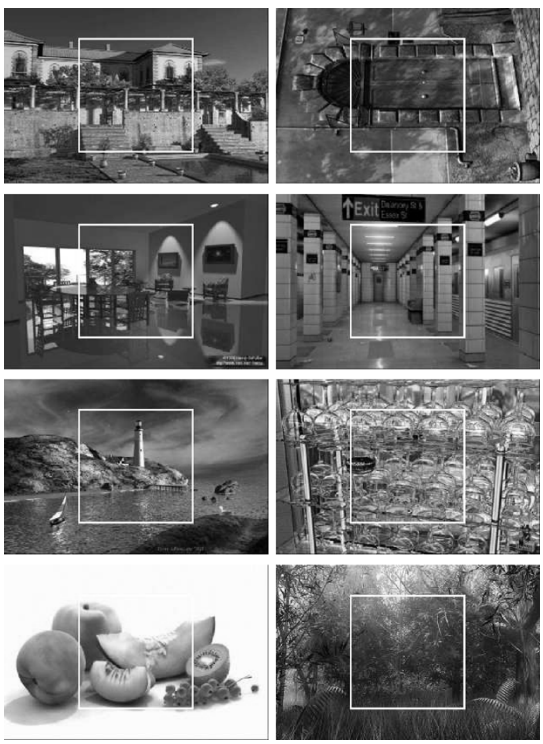

Fig. 7. Incorrectly classified photorealistic images.

website www.fakeorfoto.com. Shown in Fig. 8 are the 14 images with the correctly classified photographic images in the top row, and the correctly classified photorealistic images in the middle row. Shown in the bottom row are two incorrectly classified photographic images (left) and two incorrectly classified photorealistic images (right). Consistent with the previous results, we correctly classified 71% of the photorealistic images.

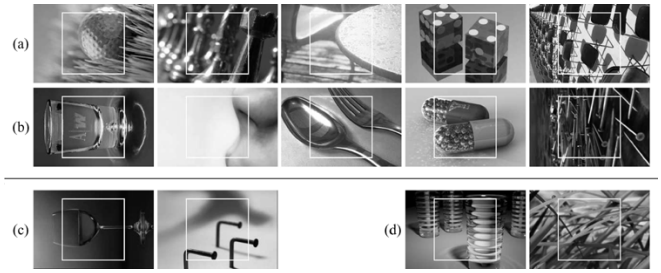

Fig. 8. Images from www.fakeorfoto.com. (a) and (c) Correctly and incorrectly classified photographic images, respectively. (b) and (d) Correctly and incorrectly classified photorealistic images, respectively.

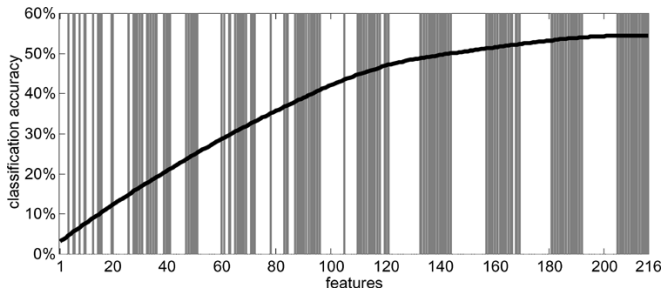

Fig. 9. Classification accuracy as a function of the number and category of feature for the LDA classifier. The white and gray regions correspond to error and coefficient features, respectively.

We wondered which set of statistics, coefficient or error, were most crucial for the classifier. Shown in Fig. 9 is the accuracy of the classifier plotted against the number and category of feature for the LDA classifier.[5] We began by choosing the single feature, out of the 216 possible coefficient and error features, that gives the best classification accuracy. This was done by building 216 classifiers each based on a single feature, and choosing the feature that yields the highest accuracy (the feature was the variance in the error of the green channel's diagonal band at the second scale). We then choose the next best feature from the remaining 215 components. This process was repeated until all features were selected. The solid line in Fig. 9 is the accuracy as a function of the number of features. The white and gray regions correspond to error and coefficient features, respectively. That is, if the feature included on the ith iteration is a coefficient then we denote that with a vertical gray line at the ith position on the horizontal axis. Note that the coefficient and error statistics are interleaved, showing that both sets of statistics are important for classification.

Finally, we attempted to retrain the nonlinear SVM with random class labels assigned to the training images. The rationale for this was to ensure that the statistical model and classifier are discriminating on fundamental differences between photographic and photorealistic images, and not on some artifact. To this end, we expect a random class assignment to lead to significantly worse classification accuracy. We generated ten different training sets containing 5000 randomly selected photographic images and 5000 photorealistic images. Half of these images were randomly assigned to the photographic class

[5]This analysis was performed only on the LDA because the computational cost of retraining $23{,}220 = 216 + \cdots + 1$ nonlinear SVMs is prohibitive. We expect the same pattern of results for the nonlinear SVM.

and the other half were assigned to the photorealistic class. We then trained nonlinear SVM classifiers on these training sets and tested them on the testing sets as used in our experiment described above. The best performance across the ten training sets was 27.6% correctly classified photographic images, with a 1.4% false-negative rate. Note that this is significantly worse than the 66.8% detection accuracy when the correct training labels were used. This result indicates that our statistical model and classifier are discriminating on fundamental statistical differences between photographic and photorealistic images.

V. Discussion

We have described a statistical model for photographic images consisting of first-order and higher order wavelet statistics. This model seems to capture regularities that are inherent to photographic images. We have also shown that this model, coupled with either an LDA or a nonlinear SVM, can be used to differentiate between photorealistic and photographic images. It is interesting to see that even though photorealistic images can be perceptually indistinguishable from photographic images, their underlying statistics can still be significantly different. These techniques are also likely to have important applications in the growing field of digital forensics.

There are, of course, several possible extensions to this work. We expect that these techniques can be extended to differentiate between synthetically generated and natural voice signals and video streams. In addition, as in earlier work [8], we expect a one-class SVM, that only requires training from photographic images, to simplify the classifier training.

Finally, we note that it is not immediately obvious that a photorealistic image could be altered to match the expected higher order statistics of photographic images. The drawback of this, from a rendering point of view, is that these models do not necessarily give any insight into how one might render more photorealistic images. The benefit, from a digital forensic point of view, is that it is likely that this model will not be immediately vulnerable to counter-attacks. It is possible, of course, that counter-measures will be developed that can foil the classification scheme outlined here. The development of such techniques will, in turn, lead to better classification schemes, and so on.

References

[1] V. Athitsos, M. J. Swain, and C. Frankel, "Distinguishing photographs and graphics on the world wide web," in *Proc. Workshop Content-Based Access Image Video Libraries*, San Juan, PR, 1997.

[2] R. W. Buccigrossi and E. P. Simoncelli, "Image compression via joint statistical characterization in the wavelet domain," *IEEE Trans. Image Processing*, vol. 8, no. 12, pp. 1688–1701, Dec. 1999.

[3] C.-C. Chang and C.-J. Lin, *LIBSVM: A Library for Support Vector Machines*, 2001.

[4] F. Cutzu, R. Hammoud, and A. Leykin, "Estimating the degree of photorealism of images: Distinguishing paintings from photographs," in *Proc. IEEE Conf. Computer Vision Pattern Recognition*, Madison, WI, 2003.

[5] R. Duda and P. Hart, *Pattern Classification and Scene Analysis*. New York: Wiley, 1973.

[6] J. Gluckman, "On the use of marginal statistics of subband images," in *Proc. IEEE Int. Conf. Computer Vision*, Nice, France, 2003.

[7] S. Lyu and H. Farid, "Detecting hidden messages using higher-order statistics and support vector machines," in *Proc. 5th Int. Workshop Information Hiding*, Noordwijkerhout, The Netherlands, 2002.

[8] ——, "Steganalysis using color wavelet statistics and one-class support vector machines," in *Proc. SPIE Symp. Electronic Imaging*, San Jose, CA, 2004.

[9] A. McNamara, "Evaluating realism," in *Proc. Perceptually Adaptive Graphics—ACM SIGGRAPH and Eurographics Campfire*, Snowbird, UT, May 2001.

[10] G. W. Meyer, H. E. Rushmeier, M. F. Cohen, D. P. Greenberg, and K. E. Torrance, "An experimental evaluation of computer graphics imagery," *ACM Trans. Graphics*, vol. 5, no. 1, pp. 30–50, 1986.

[11] P. M. Rademacher, *Measuring the Perceived Visual Realism of Images*. Chapel Hill, NC: Univ. North Carlina, 2002.

[12] E. P. Simoncelli and E. H. Adelson, *Subband Image Coding*, J. W. Woods, Ed. Norwell, MA: Kluwer, 1990, ch. Subband transforms, pp. 143–192.

[13] M. Szummer and R. W. Picard, "Indoor-outdoor image classification," in *Proc. IEEE Int. Workshop Content-Based Access Image Video Databases, in Conjunction with ICCV*, Bombay, India, 1998, pp. 42–51.

[14] A. Torralba and A. Oliva, "Semantic organization of scenes using discriminant structural templates," in *Proc. Int. Conf. Computer Vision*, Korfu, Greece, 1999.

[15] P. P. Vaidyanathan, "Quadrature mirror filter banks, M-band extensions and perfect reconstruction techniques," *IEEE Acoust., Speech, Signal Process. Mag.*, vol. 4, no. 3, pp. 4–20, Jul. 1987.

[16] A. Vailaya, A. K. Jain, and H.-J. Zhang, "On image classification: City vs. landscapes," *Int. J. Pattern Recognit.*, no. 31, pp. 1921–1936, 1998.

[17] V. Vapnik, *The Nature of Statistical Learning Theory*. New York: Spring–Verlag, 1995.

[18] M. Vetterli, "A theory of multirate filter banks," *IEEE Trans. Acoust., Speech, Signal Processing*, vol. ASSP-35, no. 3, pp. 356–372, Mar. 1987.

Siwei Lyu received the B.S. degree in information science in 1997 and the M.S. degree in computer science from Peking University, Beijing, China. He is currently pursuing the Ph.D. degree in computer science at Dartmouth College, Hanover, NH.

Hany Farid received the B.S. degree in computer science and applied mathematics from the Unversity of Rochester, Rochester, NY, in 1988 and the Ph.D. degree in computer science from the University of Pennsylvania, Philadelphia, in 1997.

He joined the faculty at Dartmouth College, Hanover, NH, in 1999, following a two-year postdoctoral position in brain and cognitive sciences at the Massachusetts Institute of Technology, Cambridge.